https://doi.org/10.1016/j.conbuildmat.2022.129020

Valorization of spent fluorescent lamp waste glass powder as an activator for eco-efficient binder materials

Hafiz Asad Ali[1], Jian Xin Lu[2], Keke Sun[3] and Chi Sun Poon[4*]

1. Ph.D. Candidate, Department of Civil and Environmental Engineering, The Hong Kong Polytechnic University, Hong Kong, Email: asad.ali@connect.polyu.hk
2. Ph.D. Candidate, Department of Civil and Environmental Engineering, The Hong Kong Polytechnic University, Hong Kong, Email: jianxin.lu@polyu.edu.hk
3. Postdoctoral Fellow, Department of Civil and Environmental Engineering, The Hong Kong Polytechnic University, Hong Kong, Email: ke-ke.sun@polyu.edu.hk
4. *Chair Professor (Corresponding author), Department of Civil and Environmental Engineering, The Hong Kong Polytechnic University, Hong Kong, Email: cecspoon@polyu.edu.hk

Abstract

Spent fluorescent lamp waste glass is considered hazardous and requires an appropriate management and recycling route. Due to its highly alkali-siliceous nature, the feasibility of using the powdered form of the fluorescent lamp waste glass (FGP) to synthesize an activator for activating the GGBS/FA blend was studied. Additionally, the solubility and reactivity of FGP were compared with waste beverage bottle glass powder (BGP). Results showed that FGP had a higher solubility and reactivity than BGP due to the presence of the higher network modifiers. A significant enhancement in solubility (about 19%), total heat release (57 – 62%), and compressive strength (85 – 89%) was observed in FGP-based mixtures, implying its potential for activator design. The mechanical and microstructural properties of the alkali-activated pastes (AAP) prepared with the FGP activators were similar to those prepared with the commercially sourced reference activator. Before activator preparation, washing FGP with water or acid enhanced the availability of soluble silicates. The activators prepared with these washed FGP accelerated the alkali-activation process and helped achieve better strengths for the corresponding AAP. Their compressive strength values were in the range of 36 – 40 MPa and comparable to the control (FGP-

C). In addition, the microstructural analysis showed that the reaction products in these mixtures were of C-(N)-A-S-H gels type with high Si/Al and low Ca/Si ratios. Thus, a recycling route for spent fluorescent lamp waste glass was preliminary demonstrated in this study.
Keywords: Fluorescent lamp waste glass; Alkali-activated material; Fly ash; Ground granulated blast furnace slag; Activator; Recycling;

1. Introduction

Due to the burgeoning demands for infrastructure developments and the achievement of carbon neutrality, the construction industry has realized that it cannot rely only on ordinary Portland cement (PC) concrete but also requires other sustainable alternative construction materials [1–4]. In this context, alkali-activated materials (AAM) are emerging alternative binders that have similar mechanical strengths and improved durability over PC-based materials if properly proportioned and cured [5,6]. In particular, the durability of AAM against acid [7], freeze-thaw [8,9], and high temperature [10] have been well established. However, there are some limitations (e.g., alkali-silica reaction (ASR), efflorescence, cost, global warming potentials etc.,) for the large-scale adoption of these materials [9,11]. According to RILEM TC 247-DTA round robin test [8], it was found that alkali-activated binders (regardless of the precursor type) when combined with non-reactive or potentially expansive aggregates caused no problematic expansion. Significant ASR expansions were observed by the highly reactive aggregates. In addition, recent studies [12–14] reported the reduction in ASR expansion of alkali-activated cement (AAC) mortars prepared using glass cullet as highly reactive aggregates and recycled glass powder and ground granulated blast furnace slag (GGBS) as binding materials through the incorporation of Al-rich materials. Such admixtures (i.e., low Ca fly ash (FA), metakaolin, calcium aluminate cement) diluted the pore solution alkalinity (the main factor of ASR in alkali-activated slags) and enhanced the strength and durability of optimal mixtures [15]. Another durability issue under debate, known as "efflorescence" in AAM, arises due to the diffusion and migration of alkali ions through the microstructure of AAM to their surface and subsequently the formation of alkali carbonates when these ions react with carbon dioxide. This phenomenon imposes potential threats of surface scaling, crystallization pressure causing internal cracking, and consequently strength reduction as indicated by previous studies [16–20]. On the contrary, some researchers [21,22] suggested that strength reduction when AAM was immersed in water was due to weaker cohesive forces between gel

particles and not due to alkalis loss. It had been reported that the role of alkalis in these systems was to dissolve precursors and did not affect the Si and Al environments if their concentrations decreased. Thus, there are different opinions among the scientific community regarding the efflorescence in AAM. However, various studies proposed different techniques to control the efflorescence in AAMs, considering many factors, including alkali metal types [21–24], raw materials [25–29], and reaction conditions [20,25] with varying degrees of success. Longhi et al. [27] reported that one of the most effective strategies to control efflorescence was increasing Si/Al in the AAC gels. Also, it was observed that the coexistence of N-A-S-H and C-A-S-H or N(C)-A-S-H gels in AAM had an inhibitory effect on efflorescence [29].

Generally, AAM are produced by alkaline activation of various natural or synthetic aluminosilicate precursors. Industrial by-products or wastes also have the potential to act as precursors, thereby providing an additional incentive to reduce the tremendous burden on landfills [30–33]. The most used precursors are GGBS, FA, MK, or a combination of these materials. The hydroxides/carbonates of alkaline metals or alkaline earth metals and $M_2O(n)SiO_2$-type siliceous salts (where M is an alkaline ion) are commonly used activators. However, the production of alkaline solutions particularly sodium silicates (one of the most effective activators), is costly and energy-intensive which requires a lot of natural resources and has adverse environmental impacts [2,34–36]. These activators can contribute as much as 90% of the total environmental impacts associated with the use of AAM [5]. Based on the life cycle assessment (LCA) of the mix proportioning of AAM, the large-scale implementation of these activators has been discouraged by some scholars [1,37,38]. Therefore, extensive field applications of AAM are still restricted. Also, Ouellet-Plamondon and Habert [1] reported that only those AAMs prepared by the "one-part" technique had lower carbon footprints than PC-based materials. The significant economic and environmental consequences associated with preparing AAM highlights the urgency of sustainable and cost-effective development of alternative activators.

After spending their service life, fluorescent lamps, regardless of whether they have undergone mercury removal, are classified as hazardous e-waste. Their global annual production is nearly 1.5 billion units [39]. In Hong Kong, a huge amount of spent fluorescent lamps are produced [40]. Even after the recovery of the valuable materials (e.g., Hg and rare earths), the waste glass associated with the fluorescent lamps requires proper management. One innovative recycling route

explored by previous studies [41,42] was to utilize this waste glass as a precursor to partially replace conventional aluminosilicates in AAM due to the lamps containing large amounts of alkali and silica, and are highly amorphous in structure. However, the resulted strength was lowered when a large amount of glass was used for a specific activator concentration, or activator to precursor ratio, and reaction conditions [32,43–45]. Similar results were also reported by Xiao et al. [46] when GGBS was replaced by waste glass powder at higher levels in alkali-activated GGBS/waste glass powder binary systems. This was attributed to insufficient Ca and Al availability in the reaction systems, resulting in lower amounts of C-(N)-A-S-H gels and related strength developments. Another possible recycling method could be by using the waste glass from spent fluorescent lamps as a silicate source to replace the water glass activator.

Previous studies described the recycling of waste beverage bottle glass and other industrial by-products or wastes rich in Si to produce silicate solutions [36,47–53]. However, due to the differences in chemical compositions among such materials and waste glass from spent fluorescent lamps [51,54,55], and this waste glass being hazardous e-waste, the feasibility of using it as an activator is scarce. Therefore, this study aimed to explore the feasibility of using waste glass from spent fluorescent lamps to replace the traditional activator (a solution of sodium metasilicate) for the activation of GGBS/fly ash blends. Besides, the solubility and reactivity of waste beverage bottle glass and waste glass from spent fluorescent lamps were assessed.

2. Materials and methods

2.1 Materials

The precursors used in this study were granulated ground blast furnace slag (GGBS) and low Ca fly ash (FA). GGBS was sourced from China (Yau Lee Wah Concrete Precast Products Company Limited, Guangdong), and FA was provided locally by a Hong Kong coal-fired power plant (CLP Power Hong Kong Limited). Waste beverage bottle glass cullet and waste glass cullet from spent fluorescent lamps were sourced from a local recycler (Laputa Eco-Construction Material Co., Ltd.) and a fluorescent treatment facility (Chemical Waste Treatment Centre (CWTC), Hong Kong), respectively. The treatment facility was designed to remove Hg from spent fluorescent lamps. After collecting both types of glass cullet, these were washed (3-5 times with tap water) to remove contaminants and ensure the user's safety (in case of fluorescent lamp waste glass cullet as it is still categorized as hazardous e-waste even after treatment in CWTC), and dried at 105ºC for 1-

day. Afterwards, these cullet were ground separately in a laboratory ball mill to obtain bottle glass powder (BGP) and fluorescent lamp waste glass powder (FGP) with an average particle size of ~10-20 μm.

FGP was further washed with distilled H_2O or 0.20M H_2SO_4 at a liquid-to-solid ratio of 20 mL/g by stirring at 800 rpm for 2 h, following the procedures described in previous studies [56,57]. Subsequently, the obtained R-FGP slurries were centrifuged and placed in an oven at 105ºC for 24 hours. Two types of FGP were obtained through this step: W-FGP was water-washed fluorescent lamp waste glass powder, whereas A-FGP was obtained after the acid washing and R-FGP was the fluorescent lamp waste glass powder without washing. The aim of washing the fluorescent lamp waste glass powder with acid was to enhance the soluble silica content ($\equiv Si{-}O^{-}H^{+}$ units) as suggested by previous studies [57,58].

The images of the raw materials used in this study are shown in Fig. A1a (see Appendix A). The chemical compositions of the raw materials are determined (Table 1) by a Rigaku Supermini200 X-ray fluorescence spectrometry. It can be seen that GGBS mostly consisted of CaO, SiO_2, and Al_2O_3, a typical hydraulic material [59], whereas FA contained SiO_2 and Al_2O_3 in abundance, indicating a type of aluminosilicate. In addition, the glasses contained mainly silica and alkalis, which might be named as alkaline-siliceous materials. No significant changes in chemical composition were observed after water or acid washing of the FGP (Table 1).

The particle size distributions (PSD) of the raw materials were analyzed using a Malvern Mastersizer 3000 particle size analyzer and are presented in Fig. A1b (see Appendix A). The X-ray diffractograms and SEM images of GGBS and FA were obtained by an X-ray diffractometer (Rigaku SmartLab 9kW – Advance) and a scanning electron microscope (Tescan VEGA3) respectively (Fig. A2, see Appendix A). The amorphous nature of BGP and FGP was reported previously [42,60,61]. Here, GGBS has an amorphous structure with a very weak peak of akermanite, detected at 31.8º. In addition, quartz and mullite were identified in FA. Moreover, no crystalline phases were observed (see Fig. A3, Appendix A) after water or acid washing for the FGP. Fig. A2b shows that GGBS and FA are made up of irregular and spherical-shaped particles, respectively. An anhydrous sodium metasilicate was used as a commercially sourced activator (2308171-5KG International Laboratory USA supplied by Advanced Technology and Industrial Co., Ltd.). It contained 50.46% Na_2O and 47.24% SiO_2 by weight with a D_{v50} of 679.5 μm. NaOH

and KOH were AR grade with 98% purity (ACCUCHEM supplied by A-Tech Global Science Limited). In addition, standard sand was used as the fine aggregate to prepare standard mortars to elucidate the reactivity of BGP and FGP.

Table 1 Chemical compositions and physical properties of raw materials

Chemical composition (%)	GGBS	FA	BGP	FGP	W-FGP	A-FGP
Na_2O			13.6	17.6	16.6	15.6
MgO	7.3	1.9	1.5	3.1	3.3	3.2
Al_2O_3	14.2	32.6	2.4	2.4	2.4	2.4
SiO_2	34.8	44.4	69.4	69.0	69.8	70.0
P_2O_5		0.4	0.2	0.1	0.1	0.1
SO_3	3.1	2.3	0.2	0.3	0.2	1.8
K_2O	0.8	1.8	0.7	1.2	1.3	1.2
CaO	38.3	6.7	10.7	4.9	5.0	4.7
Fe_2O_3	0.3	6.5	0.7	0.4	0.5	0.2
PbO				0.2	0.9	0.1
BaO				0.5	0.4	0.5
Others	1.1	1.2	0.1			
LOI		2.22	0.43	0.14		
Specific gravity	3.00	2.44	2.49	2.35		
Dv (10), μm	2.3	3.1	3.2	3.5	3.1	2.5
Dv (50), μm	12.9	12.7	9.1	9.0	7.3	5.6
Dv (90), μm	33.4	41.1	30.9	38.0	33.0	15.9

(Note: Reported are the average values of at least three observations for each material)

The step-by-step experimental plan is given below:

- Assessment of beverage bottle glass powder (BGP) and fluorescent lamp waste glass powder (FGP) in terms of solubility, total heat release and compressive strength of standard mortars prepared with a constant alkali dosage.
- From the findings above, the waste glass powder which dissolved quickly and induced a higher total heat release and compressive strength (as in the case of FGP) was used to prepare alternative activators (R/N, W/N, and A/N).
- Characterization of R/N, W/N, and A/N activators.
- Preparation of alkali-activated pastes (AAP) using GGBS and FA as precursors and alternative activators.
- Evaluation of the performance of the resulting AAP pastes and compare them with those prepared with the reference activator.

The details of each step and the related methodology were given in the following sections:

2.2 Solubility and reactivity (in terms of total heat release and compressive strength of standard mortars) of BGP and FGP

2.2.1 Solubility test

The solubility of BGP and FGP was assessed in terms of the level of Si and Al ions dissolved in 1M NaOH at a liquid-to-solid ratio of 10 mL/g. For simple comparison and based on the procedure described by previous studies [62–64] in which glass solubility in NaOH solutions increased with pH up to 14 and a higher pH resulted in slower dissolution, the authors selected 1M NaOH (pH ~ 13) to assess the potentials of both glasses. Also, the limitation of the Rigaku Supermini200 X-ray fluorescence spectrometer working at a highly alkaline environment was considered. The solution was heated at 80ºC and continuously stirred for 24 h. After cooling and filtration, the dissolved ions were measured by a Rigaku Supermini200 X-ray fluorescence spectrometry.

2.2.2 Reactivity test (total heat release and compressive strength of standard mortars)

In general, direct or indirect methods are performed to elucidate the alkaline reactivity of materials [65]. A single test cannot predict the reactivity of any material in Portland and non-Portland cement-based systems due to various factors including chemistry, mineralogical compositions, fineness, reaction extents, mix proportions, and reaction conditions. Two methods were used here to assess the BGP and FGP. For an indirect approach, standard mortars of BGP and FGP were

prepared with binder : aggregate = 1:2.75 and liquid : binder = 0.484:1, where the solid was BGP or FGP, and the liquid was 1M NaOH or KOH. The performance of AAM prepared with potassium (K) based activators were found superior to that of AAM prepared with sodium (Na) based activators, as reported previously [66]. Considering this behavior, the authors assessed BGP and FGP prepared with different alkali cationic (Na and K) environments with the aim to develop Na or K-based alternative activators subsequently. The prepared 40 mm cubic specimens were steam cured at 80ºC and tested at 7-day for compression.

Heat release is considered a prime reaction indicator that can be regarded as a direct testing scheme. Even, even in non-Portland cement-based mixtures, various studies [67–71] adopted total heat release to elucidate the reactivity and degree of reactions. For instance, an improved reactivity in terms of total heat release was reported by Kaze et al. [68] for the geopolymers prepared with halloysite clays calcined at 700 - 750ºC. Another study [67] investigated the effects of different activators (NaOH and NaOH/sodium silicate at different concentrations) on the reactivity of clay in terms of heat release. Moreover, it is practical, repeatable, and applicable to a variety of materials and correlates well with their strength developments [67,69,72]. That was why the authors considered this method for the reactivity assessment of different glass powders. For this, slurries of BGP and FGP were prepared at a liquid-to-solid ratio of 0.6 mL/g. The liquid used was 1M NaOH or KOH. About 80g of the slurries were poured into calorimetry cups, and then these were placed in the isothermal calorimeter (Calmetrix I-Cal 4000). The calorimeter was preconditioned at 40ºC, and the initial data of the first hour was discarded for signal stabilization. The total heat released from the samples for 48-hours was used for reactivity measurement.

2.3 Preparation and characterization of alternative activators

A reference activator "C" was chosen by adding the commercially sourced anhydrous sodium metasilicate to the full quantity of mixing water, keeping Na_2O-to-binder and water-to-binder ratios of 0.05 and 0.4, respectively where binder is the sum of GGBS and FA only. This solution had a pH = 13.67. In addition, the following alternative activators were prepared, keeping the same water-to-binder ratio of 0.4 and 5% Na_2O by weight of the binder:

- A mixture of R-FGP (FGP without washing) and NaOH was added to the mixing water to yield an alternative activator with a pH of 13.66, and it was denoted by R/N.

- An activating solution (denoted as W/N) with a pH of 13.74 was obtained by adding a mixture of W-FGP and NaOH to the mixing water.
- A-FGP, NaOH, were added to the mixing water to yield a potential activator (denoted as A/N) with a pH of 13.78.

The above alternative activators were sonicated at 80ºC for 24 h prior to pH testing. Heating the alternative activators at 80ºC under sonication for 24 h prior to pH testing was to 1) enhance the dissolution (reaction rates) of different fluorescent glass powders (R-FGP, W-FGP, and A-FGP) and 2) and ensure the complete dispersion of the glass powder particles (an increase of reaction surface areas) in the solutions. Moreover, the resulting solutions were allowed to cool down before pH measurements. The reference activator and the alkaline solutions derived from different fluorescent lamp glass powders were analyzed by ATR-FTIR (PerkinElmer Spectrum Two FT-IR Spectrometer).

2.4 Mix proportions and preparation of alkali-activated pastes (AAP) using GGBS and FA as precursors and alternative activators

The precursor consisted of 50% GGBS and 50% FA [73,74]. It was mixed with different activator solutions in a laboratory mixer at a higher speed for 5 minutes, and paste specimens of 40 x 40 x 40 mm in dimensions were cast. These specimens were covered with plastic sheets to avoid moisture loss after casting. After 24 h, the samples were demolded and cured in the laboratory environment (25ºC and 80 RH) for various periods before testing.

Regarding specimen IDs, "FGP-C" refers to the "control" alkali-activated pastes (AAP) made up of the reference activator "C" (commercial anhydrous sodium metasilicate), and FGP-X represents the specimens prepared with the alternative activators, where X = R/N, W/N, or A/N. R means raw-FGP (un-washed), W is water-washed FGP, and A represents the acid-washed FGP.

2.5 Testing and characterization of AAP

The compressive strength test was performed on 1-day, 7-day, and 28-day cured AAP specimens prepared with the different activators, following ASTM C109 [75]. The loading rate was kept at 0.6 MPa/s, and the average values were obtained from three observations.

After performing the compressive strength on 28-d cured samples from each mixture, the small fractured pieces from the core of the specimens were stored in ethanol for 3 days to stop the

reaction. Afterwards, these pieces were dried to remove the remnant ethanol and placed in a vacuum dryer at 40°C until microstructural testing and TG measurement.

For XRD testing, these small dried pieces were ground using mortar and pestle, and the fraction passing through 45 μm, was used. The phases in the samples were identified by Rigaku SmartLab 9kW – Advance X-ray diffractometer. The scan range of 10-70° 2θ was set with a step size of 0.03°/s, and recording was done with Cu-Kα radiation (λ~1.54 Å). Besides, XRD patterns of washed fluorescent lamp glass powder with water or acid were also recorded.

For ATR-FTIR analysis of the powdered samples (particle size < 45μm), PerkinElmer Spectrum Two FT-IR Spectrometer was used, and IR spectra were obtained in the wavelength range of 4000–400 cm^{-1} after running 64 scans.

For SEM-EDX analysis, the dried powdered sample obtained from each 28-d ambient cured paste was used. SEM sample was prepared by placing the powdered sample on an SEM pin stub with the help of conductive carbon tape, followed by sputtering with a gold coating for conduction purposes, and then observed under Tescan Vega3 scanning electron microscope equipped with energy dispersive x-ray analyzer.

TG measurements were performed using a Rigaku Thermo Plus EVO2 Thermalgravimetry Analyser (TGA) in the temperature range of 30 – 1000°C with a heating rate = 10°C/minute.

3. Results and discussion

3.1 Solubility of BGP and FGP

Table 2 shows that the dissolution of FGP was higher than BGP at 80°C in 1M NaOH (pH ~ 13) and was due to the presence of more glass modifiers (Na_2O_{eq} + PbO) and fewer glass stabilizers (CaO + MgO) in FGP compared to BGP. The values of network modifiers and glass stabilizers for FGP vs. BGP (measured by X-ray fluorescence spectrometry) were 18.6 vs. 14.1, and 8.1 vs. 12.2, respectively. This indicated that glass dissolution is strongly influenced by its oxide composition [54].

It can be further explained by the field strength values of their various oxides. Field strength value, denoted by F and equals ion valence divided by the ionic distance for oxide, is related to the cation-oxygen bond strength. Usually, the glass formers i.e., SiO_2 and Al_2O_3 have F > 1.3, and the network

modifier ions have F < 0.4, whereas F equals 0.33 and 0.45 for CaO and MgO, respectively. This means that the presence of more glass formers (SiO_2 and Al_2O_3) and stabilizers (CaO + MgO), compared to network modifiers Na_2O_{eq} and PbO, such as in the case of BGP, makes the glass more stable and hence difficult to be dissolved [76]. This enhanced dissolution of FGP compared to BGP can be beneficial to design an alternative activator.

Table 2 Solubility test results, glass formers, stabilizers, and network modifiers of BGP and FGP measured by XRF spectroscopy

Properties		Type of raw material	
		BGP	FGP
Dissolution in 1M NaOH for 24 h (mass %) (at 80°C)	Si	1.3±0.1	1.6±0.9
	Al	ND	0.04±0.03
Glass formers	$SiO_2 + Al_2O_3$	71.8	71.4
Stabilizers	CaO + MgO	12.2	8.1
Network modifiers	Na_2O_{eq} + PbO	14.1	18.6

(Note: the precision up to second decimal places for Al ions was considered due to its low concentration)

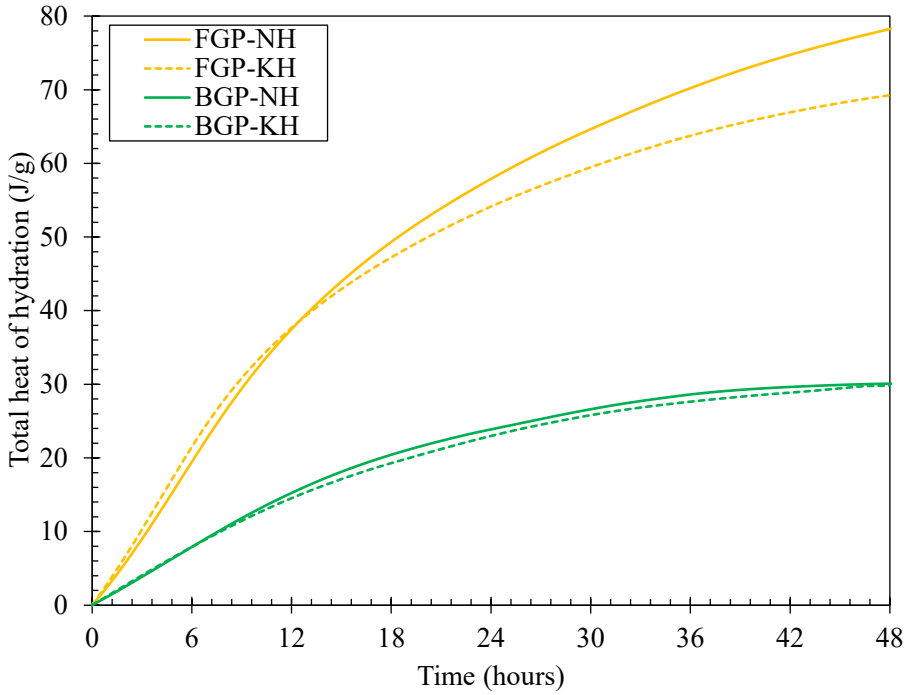

a)

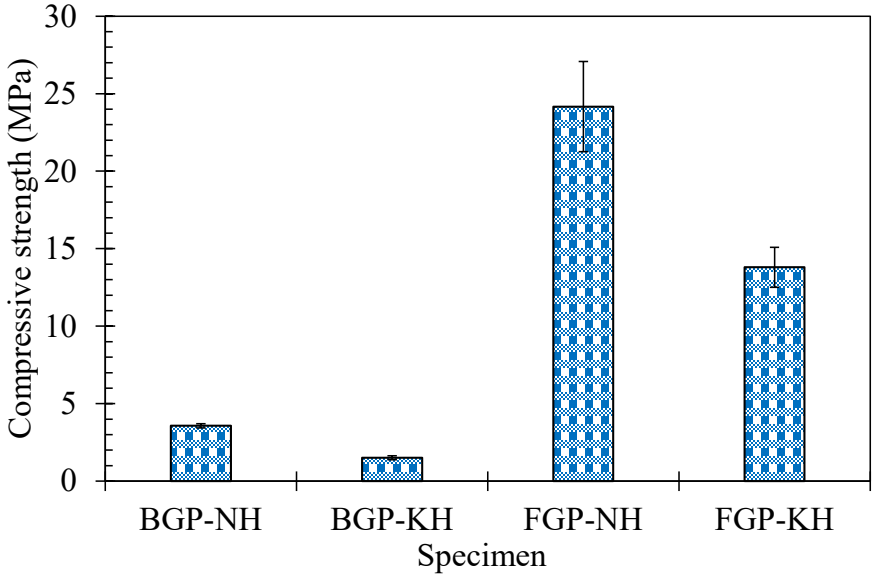

b)

Fig. 1 a) Total heat release for 48 hours, and b) compressive strength development of BGP and FGP based alkali-activated materials at the age of 7-day

3.2 Reactivity of BGP and FGP

3.2.1 Total heat release

Fig. 1a shows the total heat release for the two types of glass under different alkali cation hydroxides measured for 48 hours. Regardless of the alkali metal ion type, FGP recorded higher heat release values than BGP. Besides, the effect of NaOH was more pronounced than that of KOH at such a concentration. FGP had heat release values of 78.2 and 69.3 J/g for NaOH and KOH, respectively. On the other hand, heat release values for BGP under NaOH and KOH were 30.1 and 29.8 J/g, respectively, indicating the insignificant impact of different alkali cation hydroxides on this glass. Although, their corresponding compressive strengths were significantly different (see Section 3.2.2). This behavior might be attributed to differences in the synthesis temperature and alkalinity of the activator solutions. For the measurement of compressive strengths of the standard mortars, the curing temperature was 80ºC which enhanced the reaction rates compared to the total heat release testing operated at 40ºC. Moreover, glass solubility is highly influenced by the pH of the activator solution according to the literature [62–64]. A higher pH (as in the case of KOH) resulted in slower dissolution due to the formation of reaction products around the glass powder grains, disrupting the reaction. Overall, FGP showed a better reactivity under a low concentration of the activating solution.

3.2.2 Strength development

Like heat release, the standard mortars prepared with FGP showed better strength development than BGP at 7-days (Fig. 1b). This behavior was attributed to the presence of more glass modifiers in FGP.

The function of network modifiers is to alter the glass structure and produce non-bridging oxygens (NBOs) by depolymerizing the Si-O-Si species. The more the network modifiers, the higher the NBO sites. These NBO sites possess negative charges balanced by the network modifier ions. However, due to lower bond energies between the network modifiers and oxygen atoms, the breakage of such bonds in glass under an alkaline environment is much faster than Si-O-Si species [76,77]. Consequently, a higher dissolution may occur. This phenomenon was observed in the solubility test results of FGP. Such increased dissolution promoted the gels formation through polycondensation, resulting in a better strength achievement. Thus, the chemical composition of different glasses with nearly equal particle sizes (see Table 1) impacted the strength development.

Furthermore, regardless of the type of glass, the results indicated that at a low concentration of the activating solution, glass showed better reactivity under NaOH than KOH. This result agreed with a previous study [43]. Afterwards, we designed Na-based alternative activators using FGP.

In non-Portland cement-based mixtures, a good relationship between the total heat release and the strength development was found by previous studies [67–71]. Ling et al. [69] developed linear correlations (R^2 value ranging from 0.78 to 0.84) between total heat and compressive strength of high Ca FA-based geopolymers mixes depending on the liquid activator-to-fly ash mass ratio. For a given liquid activator-to-fly ash mass ratio, the compressive strength increased with the increase of total heat release. Similar findings were also observed by Ogundiran and Kumar [67]. However, in the present study, a reliable relationship between the total heat release and compressive strength cannot be developed due to limited data points. It is therefore recommended to incorporate a larger data set for reliable and acceptable correlations. Based on the solubility and reactivity results, FGP performed better than BGP and had a potential for synthesizing alternative activators.

3.3 Characteristics of alkaline solution derived from various FGP

Fig. 2 shows the IR spectra of the reference "C" and synthesized alkaline solutions measured by the ATR method. All the activators showed a broad -OH stretching vibration band around 3200-3400 cm^{-1}, corresponds to the molecularly adsorbed H_2O and hydrogen bonding. The peak at approximately 1644 cm^{-1} was attributed to H-O-H bending vibrations [78,79]. Besides the vibrational modes of absorbed water, two more ranges were observed in FTIR spectra of the activating solutions, i.e., range (I) from 900 to 1000 cm^{-1} and range (II) at around 415-435 cm^{-1}. Range (I) was attributed to non-symmetric stretching vibrations of Si-O-Si bonds of the SiQ^n structural units, whereas range (II) indicates the presence of asymmetric vibrations of Si-O-Si due to bending. The characteristic peaks at 973, 974, and 984 cm^{-1} indicated the presence of both SiQ^1 and SiQ^2 units [80]. However, a lower value of wavenumber could be related to the predominance of SiQ^1 units. The weak intensities at 912, 919, 921, and 922 cm^{-1} in the FTIR spectra were ascribed to SiQ^0 units. These units are considered more reactive than any other SiQ^n units and attributed to Si-O-Ca containing NBO [50,81]. The results show that the activating solutions derived from various fluorescent glass powders had similar characteristics to the reference activator and could be used for alkali activation.

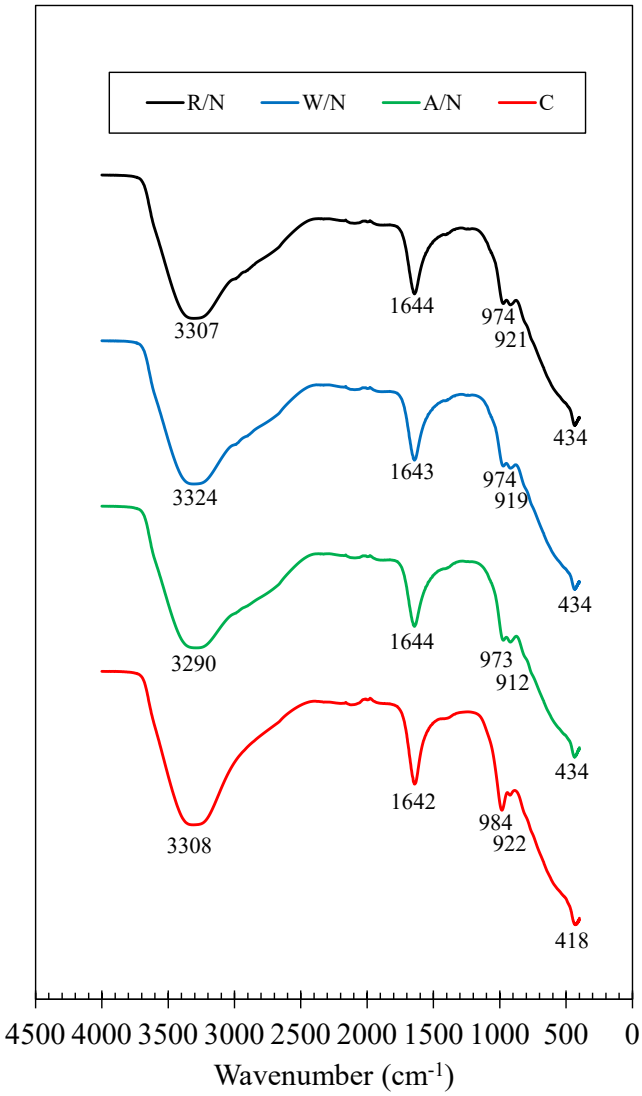

Fig. 2 FTIR spectra of alkaline solutions

3.4 Characteristics of alkali-activated pastes (AAP)

3.4.1 Compressive strength

Fig. 3 shows the compressive strength development of alkali-activated pastes (AAP) at various ages. The increase of compressive strength with curing time was observed in all the AAP. AAP prepared with R/N as an alternative activator showed the lowest strength values among all tested pastes at all ages. At an early age, pastes prepared with alternative activators showed lower strength development when compared to FGP-C, which was prepared with a reference activator. However, AAP pastes prepared with W/N and A/N activating solutions (i.e., FGP-W/N and FGP-A/N)

showed better strength development than those prepared with FGP-R/N. The specimen prepared with FGP-A/N had a similar strength value to FGP-C at a later age. This beneficial behavior was associated with water or acid washing of the fluorescent lamp glass powder prior to activator synthesis.

Diffusion of H^+ or H_3O^+ from water or acid into the glass powder extracted the alkali metal and alkaline earth ions through the ion exchange and resulted in the formation of gels (≡Si─O^-H^+ units) (Eq 1 and 2) [57,64]. As reported previously [82], this process becomes significant particularly at low pH environment.

$$\equiv Si - O^- NaO^+ + H^+ \rightarrow \equiv Si - O^- H^+ + Na^+ \quad (1)$$

$$\equiv Si - O^- Ca^{2+-} O + 2H^+ \rightarrow 2 \equiv Si - O^- H^+ + Ca^{2+} \quad (2)$$

When W-FGP or A-FGP were mixed with NaOH to synthesize W/N or A/N, these ≡Si─O^-H^+ units with the additional silicate species formed from the hydrolysis of W-FGP or A-FGP at high pH were present in these activators. Thus, the cumulative amount of soluble silicate species was responsible for accelerating the reaction and formation of reaction products, resulting in a strength increase in these pastes compared to AAP prepared with R/N. Another reason might be the refinement of particle sizes after water or acid washing that enhanced the reactive surfaces of the silicate species during the activator preparation. Consequently, such activators (i.e., W/N or A/N) promoted the alkali-activation process and achieved better strength development.

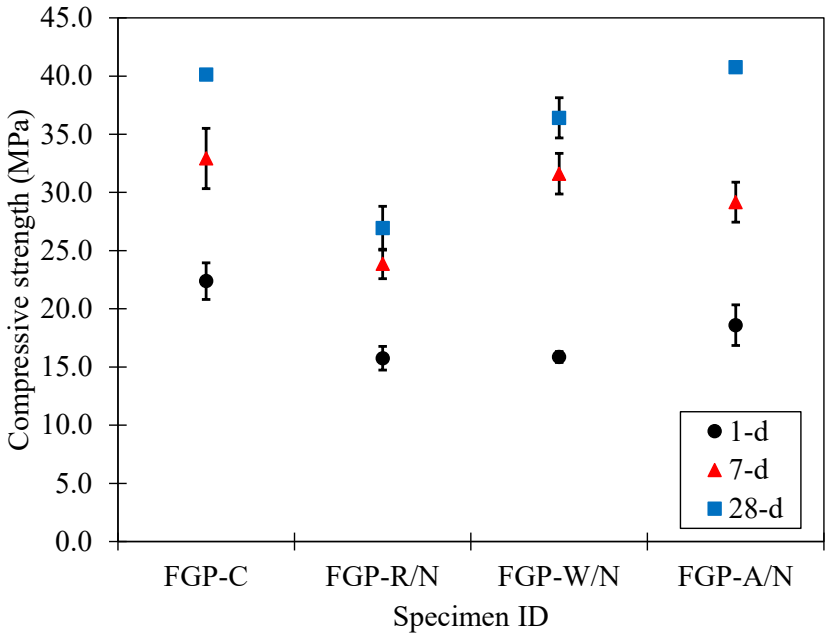

Fig. 3 Compressive strength developments of AAP prepared with different activators (Note: The error bars for the "FGP-C" at 1-day and "FGP-A" at 28-days are too small to be shown)

3.4.2 Mineralogical characterization

The mineralogical characterization of all the pastes prepared with different activators and cured for 28 days was measured by XRD analysis, and the results are depicted in Fig. 4a. No mineralogical changes were observed, indicating that the reaction products of all the investigated mixtures were similar. In all the tested pastes, the XRD patterns indicated the presence of poorly crystalline calcium silicate hydrate (CSH) phases at a 2θ of about 29.4°. Such gel phases were reported previously [83,84] as the primary reaction product in the alkali-activated GGBS/FA pastes. Moreover, these CSH gels may contain aluminum and sodium in their structure. Puertas et al. [83,85] also detected calcium silicate hydrates that are rich in Al and included Na in the structure network of alkali-activated FA/GGBS pastes.

3.4.3 Infrared spectroscopy

Fig. 4b shows the infrared spectroscopy results of various AAP cured for 28 days. Two characteristic peaks were observed in all the pastes near the wavenumber values of around 950 and 445 cm^{-1}, ascribing to the T-O (where T = Si or Al) nonsymmetric stretching and bending vibration bands, respectively. These bands have been widely reported in alkali-activated cement (AAC) gels

and the wavenumber value at around 950 cm^{-1} indicates the presence of Si-O-Si bonds of SiQ^2 groups, which represent the structure of aluminosilicate chains consisting of aluminum-substituted C-S-H, as reported previously [80,81,84,86,87]. It can be seen that the position of this band was shifted towards a higher wavenumber in FGP-A/N compared to other AAP. This implies that more Si was incorporated into the AAC gel networks, and a higher degree of polymerization and/or silica network cross-linking was achieved (as observed in C-S-H gel phases of cementitious materials), which might be responsible for the higher strength development of the paste prepared with activator A/N. These results are in good agreement with previously published literature [84,88,89]. Furthermore, reduction of Si-O-Si in-plane bending band [50] at about 445 cm^{-1} was observed in FGP-A/N, suggesting that more silica was available for reaction to form AAC gels. Based on the FTIR data, it can be inferred that the alternative activator could develop similar types of reaction gels (e.g., C-A-S-H or C-(N)-A-S-H) as observed in the control.

3.4.4 SEM/EDX analysis

In all the tested pastes, AAP prepared with R/N showed a porous morphology responsible for its lower strengths (Fig 4c). The matrices were denser in FGP-W/N and FGP-A/N, and the specimen FGP-A/N showed a similar compactness to that of the control. Due to its small particle size, it might act as a micro-filler and provide enhanced nucleation sites during the alkali-activation, resulting in the higher strength of FGP-A/N.

EDX analysis was performed on multiple randomly selected points of the matrices of each AAP (excluding the unreacted particles) to assess the elemental compositions of the reaction products. The average values of the elemental analysis are reported in Table 3. The data shows that reaction products mainly composed of calcium, silica, sodium, and aluminum in all the tested AAP. XRD and FTIR results indicated the main reaction product was C-S-H gel. However, the presence of Al and Na, as confirmed by EDX analysis, also suggested that these C-S-H gels contained Al and Na in their structures, possibly forming C-(N)-A-S-H type of gels [83–85,90]. Moreover, the increased Si/Al ratio in FGP-A/N samples agreed with FTIR results.

Moreover, Ca/Si ratio was decreased in FGP-A/N compared to that of control (FGP-C). This agreed with the findings provided by Dai et al. [91] when they produced AAM with a SF-based activator. Such reduction was attributed to increased silicate species in the mixtures. An increase in the binding property and mean chain length of C-S-H with the decrease in Ca/Si ratio was

reported by previous studies [91–93]. Such increased Si/Al and decreased Ca/Si ratios suggested that a higher degree of polymerization and/or cross-linking of the silicate species within this matrix (FGP-A/N) might exist. Consequently, enhanced strength was obtained compared to AAP prepared with other alternative activators.

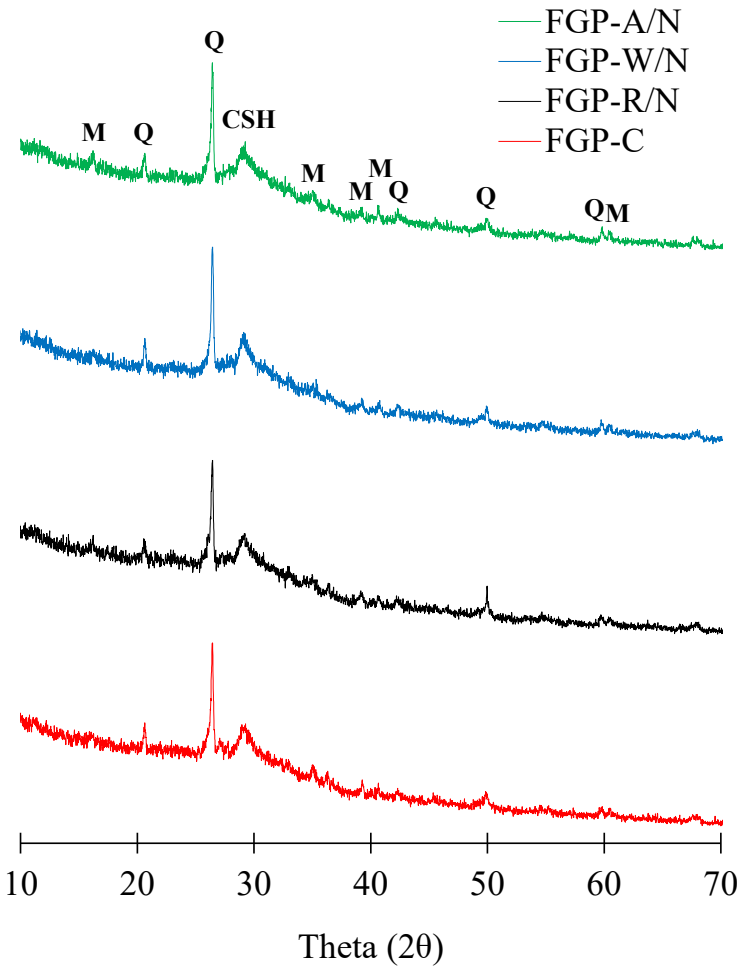

a)

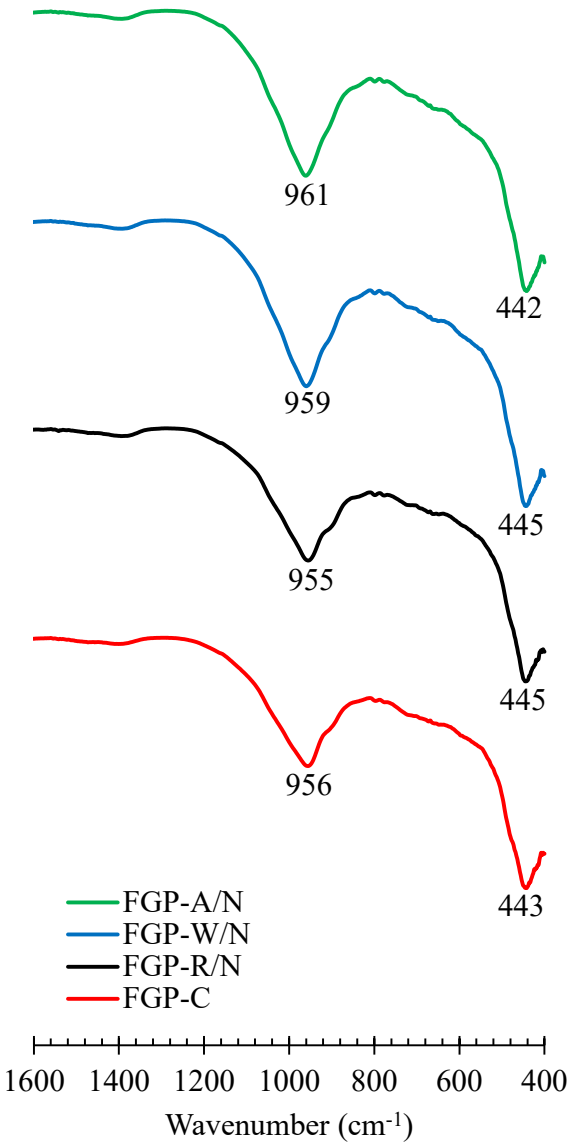
961
442
959
445
955
445
956
443
FGP-A/N
FGP-W/N
FGP-R/N
FGP-C
1600 1400 1200 1000 800 600 400
Wavenumber (cm-1)

b)

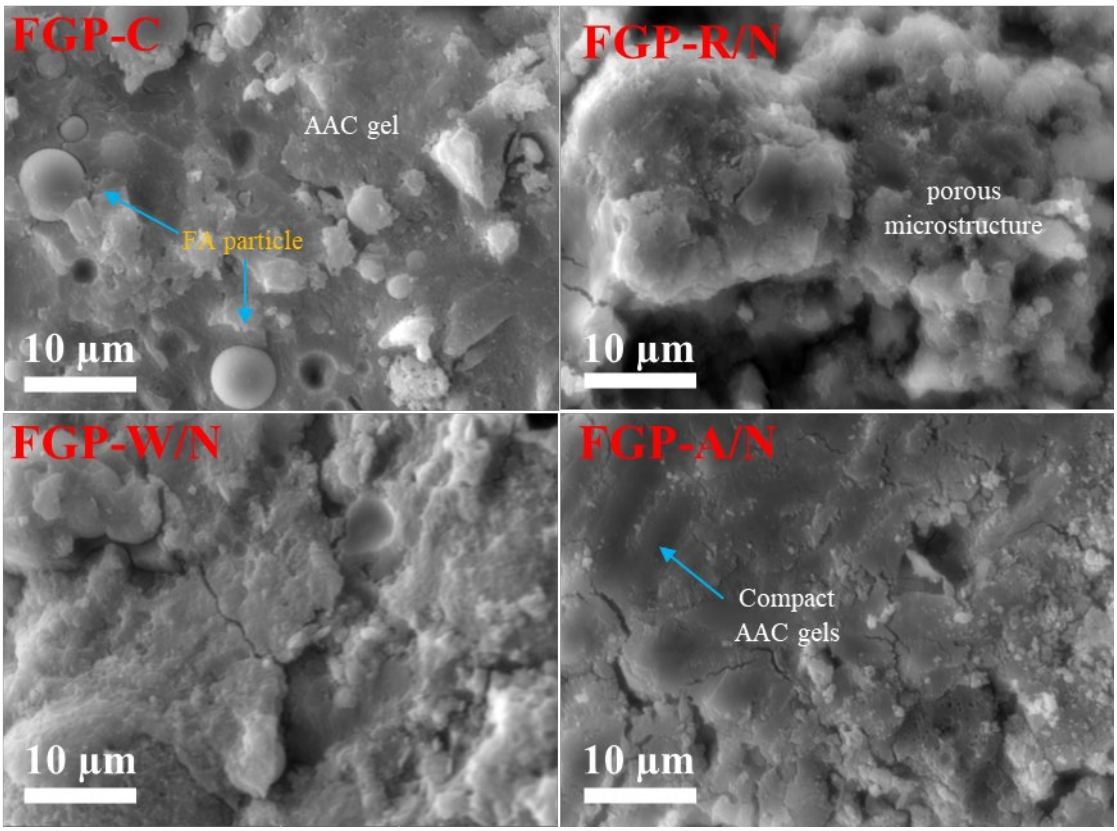

c)

Fig. 4 Characteristics of 28-d cured AAP; a) XRD spectra (M=mullite, Q=quartz, and CSH=calcium silicate hydrate), b) FTIR spectra, and c) SEM images at the approximately same magnification

Table 3 Atomic ratios of 28-d cured AAP measured by SEM-EDX analysis

Specimen ID	Atomic ratios (%)						Si/Al ratio	Ca/Si ratio
	Na	Mg	Al	Si	Ca	Fe		
C	29.51	2.45	12.52	35.02	19.58	0.91	2.80	0.56
R-FGP	5.63	4.48	15.37	41.21	29.80	3.50	2.68	0.72
W-FGP	15.72	3.32	18.82	44.35	15.43	2.35	2.36	0.35
A-FGP	22.46	4.96	15.06	44.62	11.66	1.24	2.96	0.26

3.5 Thermogravimetric analysis

Fig. 5 shows the weight loss results of AAP cured for 1 day and 28 days, measured by TGA. The results were analyzed based on two temperature ranges, starting from 50 to 250ºC and the other from 250 to 500ºC, which might be attributed to the loss of bound water from C-A-S-H or N-A-S-H phases, and the decomposition of hydroxyl (OH) groups in hydrotalcite (Ht) respectively, on the TGA curves (see Fig. 5c) [46,94]. As expected, at 1-d age, AAP pastes prepared with the alternative activators showed lower mass losses at these temperature ranges than the control, implying that these specimens contained a lesser amount of reaction gels due to the slower reactivity [82,95–97]. However, at 1-d age, FGP-W/N and FGP-A/N showed higher weight losses than FGP-A/N. At a later age (i.e., 28-d), the mass losses of FGP-W/N and FGP-A/N were similar to that of FGP-C, indicating a similar amount of reaction gels in their matrices. These results are in good agreement with their strength values.

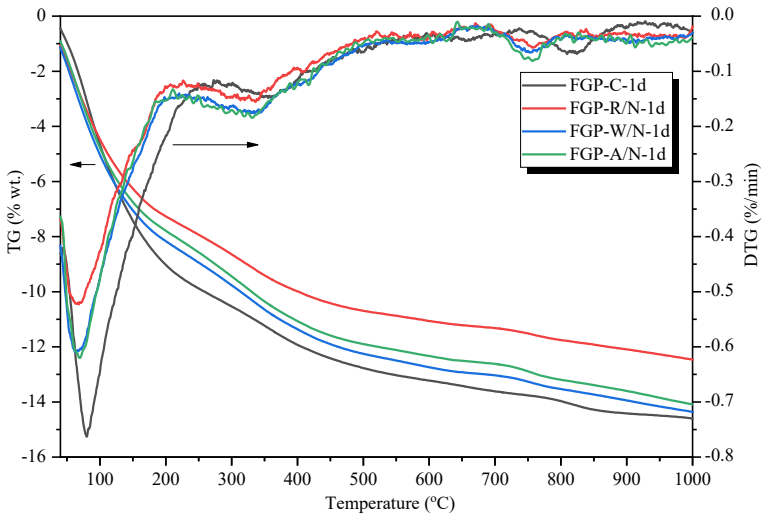

a)

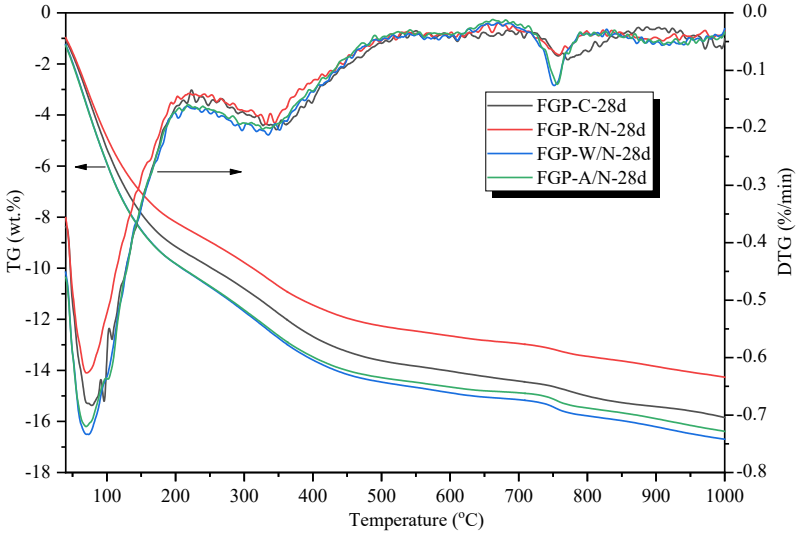

b)

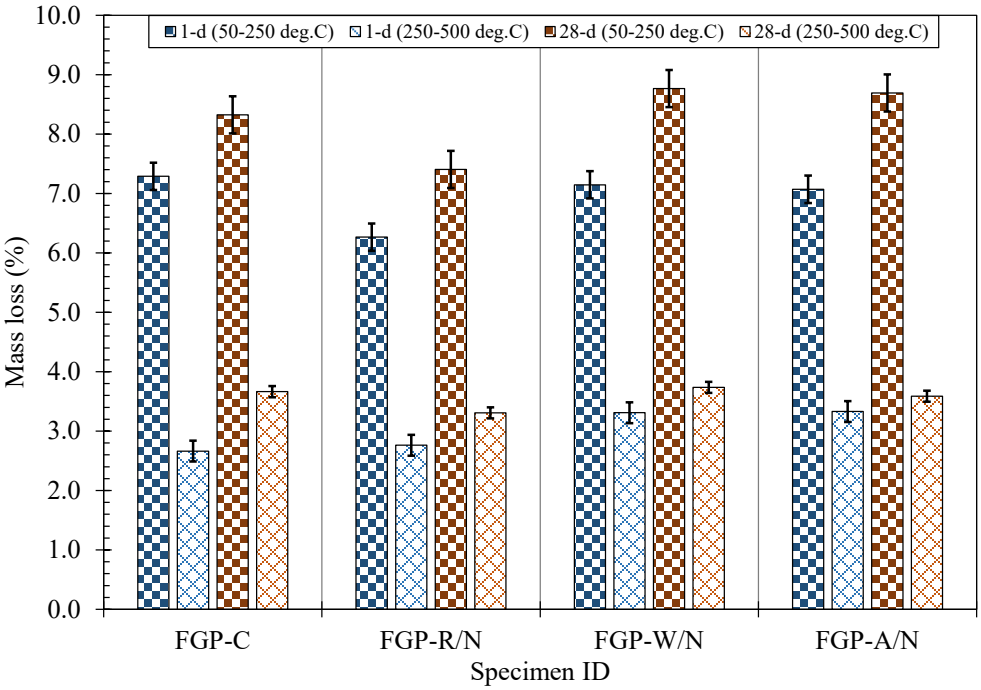

c)

Fig. 5 TG and DTG graphs at a) 1-d, b) 28-d, and c) mass loss at different ages between 50 - 250°C and 250 - 500°C of AAP measured by TGA

4. Conclusions

The following conclusions can be drawn from this study:

- The solubility of FGP in terms of Si and Al ions release was higher than that of BGP. This increase in solubility was about 19% due to more network modifiers in FGP (FGP =18.6 vs. BGP = 14.1). Such a higher amount of network modifiers had lower field strength values (F < 0.4) that eased the dissolution.
- FGP had a better reactivity than BGP regarding compressive strength and total heat release. An increase of about 85 - 89% in compressive strength and 57 - 62% in total heat release values when Na/K-based activators were used for FGP-based mixtures. This enhanced reactivity might be attributed to weaker bonds between the negatively charged NBO and modifiers than Si-O-Si bonds present in FGP. These weak bonds were easily broken in the alkaline solutions, promoting higher dissolution and gels formation through polycondensation. Consequently, a better performance was achieved. This shows its potential to be used as an alternative activator.
- Treatment of FGP with water or acid enhanced the reaction surfaces of the silicate species (presence of more SiQ^0 groups between 910 – 920 cm^{-1} at the FTIR spectra) due to the refinement of particle sizes. Such activators accelerated the alkali-activation process and achieved better strength development. The strength values were in the range of 36 – 40 MPa and comparable to the control (FGP-C).
- This work demonstrated that the waste FGP can be recycled to synthesize an environmentally-friendly activator for alkali-activated cement manufacturing. Future recommendations include the environmental and durability assessments of the AAM prepared with such alternative activators.

Conflict of interest

None.

Acknowledgments

The authors would like to thank the Research Grants Council General Research Fund for financial support.

Appendix A

Fig. A1

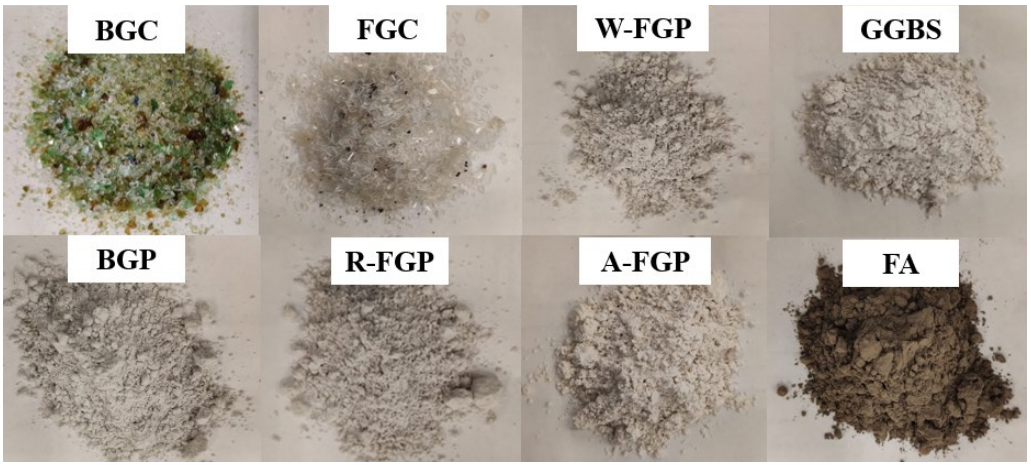

a)

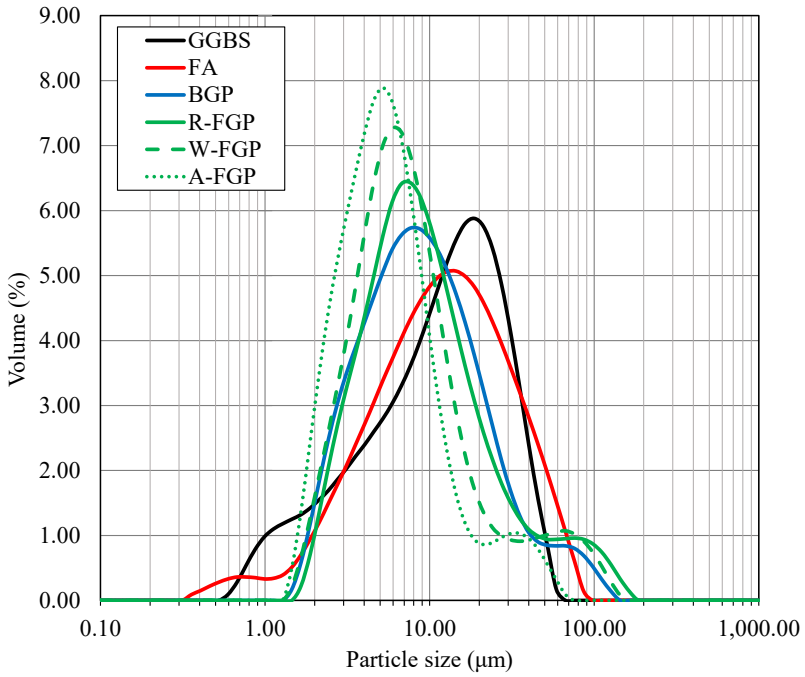

b)

Fig. A1 a) Images and b) particle size distributions of raw materials used in this study

Fig. A2

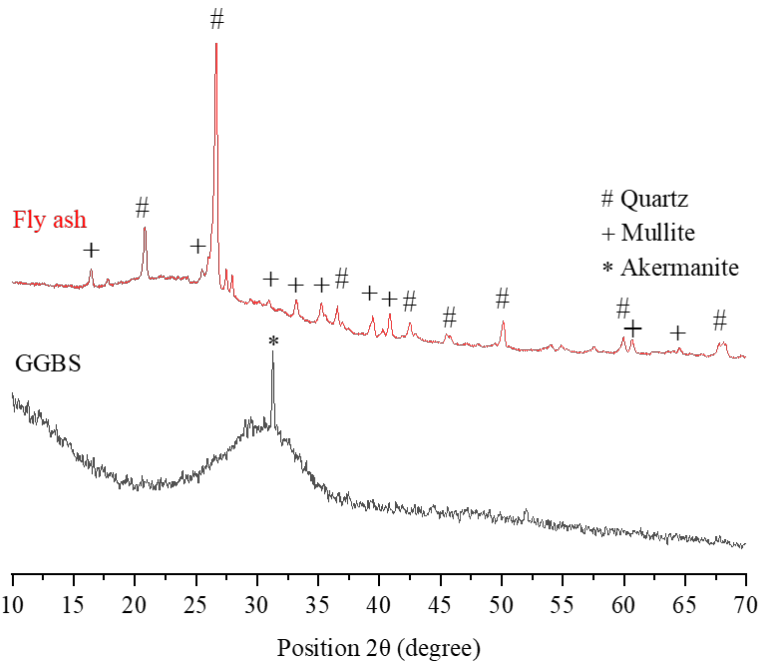

a)

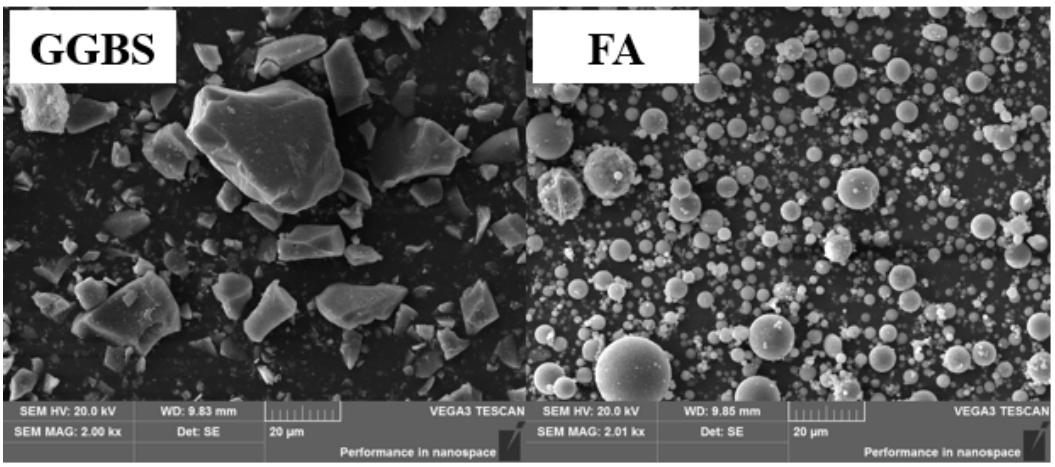

b)

Fig. A2 Characterization of GGBS and FA a) XRD patterns and b) SEM images at 2000x

Fig. A3

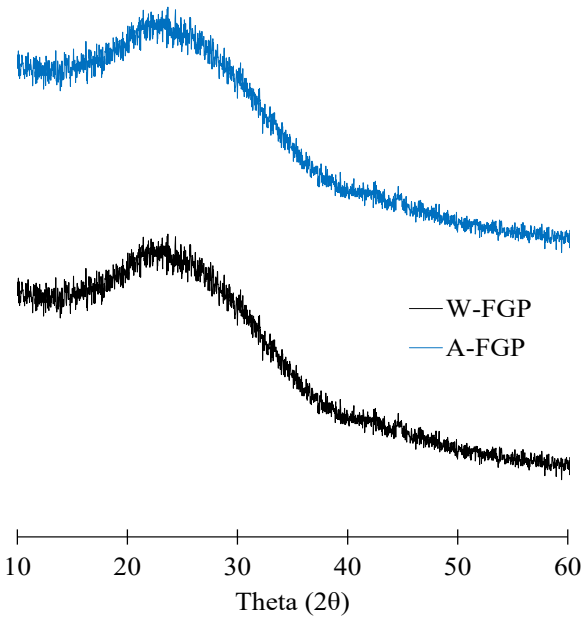

Fig. A3 XRD patterns of W-FGP and A-FGP

Abbreviations

BGC	*waste beverage bottle glass cullet*
BGP	*waste beverage bottle glass powder*
FGC	*waste glass cullet from spent fluorescent lamps*
FGP	*fluorescent lamp waste glass powder*
R-FGP	*un-washed fluorescent lamp waste glass powder (FGP and R-FGP are same)*
W-FGP	*water-washed fluorescent lamp waste glass powder*
A-FGP	*acid-washed fluorescent lamp waste glass powder*
FA	*low Ca fly ash*
GGBS	*granulated ground blast furnace slag*
C	*solution of anhydrous sodium metasilicate and water keeping Na_2O-to-binder and water-to-binder ratios of 0.05 and 0.4, respectively*
R/N	*activating solution prepared with R-FGP and NaOH*
W/N	*activating solution prepared with W-FGP and NaOH*
A/N	*activating solution prepared with A-FGP and NaOH*
FGP-C	*alkali-activated pastes (AAP) prepared with reference activator "C"*
FGP-R/N	*AAPs prepared with R/N*

526 *FGP-W/N* *AAP prepared with W/N*
527 *FGP-A/N* *AAP prepared with A/N*
528

529 References

530 [1] C. Ouellet-Plamondon, G. Habert, 25 - Life cycle assessment (LCA) of alkali-activated
531 cements and concretes, in: F. Pacheco-Torgal, J.A. Labrincha, C. Leonelli, A. Palomo,
532 P.B.T.-H. of A.-A.C. Chindaprasirt Mortars and Concretes (Eds.), Woodhead Publishing,
533 Oxford, 2015: pp. 663–686. https://doi.org/https://doi.org/10.1533/9781782422884.5.663.

534 [2] I. Bianco, B. Ap Dafydd Tomos, R. Vinai, Analysis of the environmental impacts of
535 alkali-activated concrete produced with waste glass-derived silicate activator – A LCA
536 study, J. Clean. Prod. 316 (2021) 128383.
537 https://doi.org/https://doi.org/10.1016/j.jclepro.2021.128383.

538 [3] F. Pacheco-Torgal, Z. Abdollahnejad, S. Miraldo, M. Kheradmand, Chapter 9 - Alkali-
539 Activated Cement-Based Binders (AACBs) as Durable and Cost-Competitive Low-CO2
540 Binder Materials: Some Shortcomings That Need to be Addressed, in: A. Nazari,
541 J.G.B.T.-H. of L.C.C. Sanjayan (Eds.), Butterworth-Heinemann, 2017: pp. 195–216.
542 https://doi.org/https://doi.org/10.1016/B978-0-12-804524-4.00009-9.

543 [4] G. Habert, C. Ouellet-Plamondon, Recent update on the environmental impact of
544 geopolymers, RILEM Tech. Lett. 1 (2016) 17–23.
545 https://doi.org/10.21809/rilemtechlett.2016.6.

546 [5] J.L. Provis, Alkali-activated materials, Cem. Concr. Res. 114 (2018) 40–48.
547 https://doi.org/https://doi.org/10.1016/j.cemconres.2017.02.009.

548 [6] S.A. Bernal, J.L. Provis, Durability of alkali-activated materials: Progress and
549 perspectives, J. Am. Ceram. Soc. 97 (2014) 997–1008. https://doi.org/10.1111/jace.12831.

550 [7] P. Sturm, G.J.G. Gluth, C. Jäger, H.J.H. Brouwers, H.-C. Kühne, Sulfuric acid resistance
551 of one-part alkali-activated mortars, Cem. Concr. Res. 109 (2018) 54–63.
552 https://doi.org/https://doi.org/10.1016/j.cemconres.2018.04.009.

553 [8] F. Winnefeld, G.J.G. Gluth, S.A. Bernal, M.C. Bignozzi, L. Carabba, S. Chithiraputhiran,

A. Dehghan, S. Dolenec, K. Dombrowski-Daube, A. Dubey, V. Ducman, Y. Jin, K. Peterson, D. Stephan, J.L. Provis, RILEM TC 247-DTA round robin test: sulfate resistance, alkali-silica reaction and freeze–thaw resistance of alkali-activated concretes, Mater. Struct. 53 (2020) 140. https://doi.org/10.1617/s11527-020-01562-0.

[9] F. Pacheco-Torgal, Z. Abdollahnejad, A.F. Camões, M. Jamshidi, Y. Ding, Durability of alkali-activated binders: A clear advantage over Portland cement or an unproven issue?, Constr. Build. Mater. 30 (2012) 400–405. https://doi.org/https://doi.org/10.1016/j.conbuildmat.2011.12.017.

[10] D. Panias, E. Balomenos, K. Sakkas, 16 - The fire resistance of alkali-activated cement-basedconcrete binders, in: F. Pacheco-Torgal, J.A. Labrincha, C. Leonelli, A. Palomo, P.B.T.-H. of A.-A.C. Chindaprasirt Mortars and Concretes (Eds.), Woodhead Publishing, Oxford, 2015: pp. 423–461. https://doi.org/https://doi.org/10.1533/9781782422884.3.423.

[11] J.S.J. Van Deventer, J.L. Provis, P. Duxson, Technical and commercial progress in the adoption of geopolymer cement, Miner. Eng. 29 (2012) 89–104. https://doi.org/https://doi.org/10.1016/j.mineng.2011.09.009.

[12] P. He, B. Zhang, J.-X. Lu, C.S. Poon, ASR expansion of alkali-activated cement glass aggregate mortars, Constr. Build. Mater. 261 (2020) 119925.

[13] P. He, B. Zhang, J.-X. Lu, C.S. Poon, Reaction mechanisms of alkali-activated glass powder-ggbs-CAC composites, Cem. Concr. Compos. 122 (2021) 104143. https://doi.org/https://doi.org/10.1016/j.cemconcomp.2021.104143.

[14] Z. Shi, C. Shi, J. Zhang, S. Wan, Z. Zhang, Z. Ou, Alkali-silica reaction in waterglass-activated slag mortars incorporating fly ash and metakaolin, Cem. Concr. Res. 108 (2018) 10–19. https://doi.org/https://doi.org/10.1016/j.cemconres.2018.03.002.

[15] H.A. Ali, D. Xuan, J.-X. Lu, C.S. Poon, Enhancing the resistance to microbial induced corrosion of alkali-activated glass powder/GGBS mortars by calcium aluminate cement, Constr. Build. Mater. 341 (2022) 127912. https://doi.org/https://doi.org/10.1016/j.conbuildmat.2022.127912.

[16] X. Yao, T. Yang, Z. Zhang, Compressive strength development and shrinkage of alkali-

582 activated fly ash–slag blends associated with efflorescence, Mater. Struct. 49 (2016)
583 2907–2918. https://doi.org/10.1617/s11527-015-0694-3.

584 [17] K. Arbi, M. Nedeljković, Y. Zuo, G. Ye, A Review on the Durability of Alkali-Activated
585 Fly Ash/Slag Systems: Advances, Issues, and Perspectives, Ind. Eng. Chem. Res. 55
586 (2016) 5439–5453. https://doi.org/10.1021/acs.iecr.6b00559.

587 [18] M.A. Longhi, Z. Zhang, E.D. Rodríguez, A.P. Kirchheim, H. Wang, Efflorescence of
588 Alkali-Activated Cements (Geopolymers) and the Impacts on Material Structures: A
589 Critical Analysis, Front. Mater. 6 (2019). https://doi.org/10.3389/fmats.2019.00089.

590 [19] Z. Zhang, J.L. Provis, X. Ma, A. Reid, H. Wang, Efflorescence and subflorescence
591 induced microstructural and mechanical evolution in fly ash-based geopolymers, Cem.
592 Concr. Compos. 92 (2018) 165–177.

593 [20] Z. Zhang, J.L. Provis, A. Reid, H. Wang, Fly ash-based geopolymers: The relationship
594 between composition, pore structure and efflorescence, Cem. Concr. Res. 64 (2014) 30–
595 41. https://doi.org/https://doi.org/10.1016/j.cemconres.2014.06.004.

596 [21] F. Škvára, V. Šmilauer, P. Hlaváček, L. Kopecký, Z. Cilova, A weak alkali bond in (N,
597 K)–A–S–H gels: evidence from leaching and modeling, Ceramics-Silikaty. 56 (2012)
598 374–382.

599 [22] F. Škvára, L. Kopecký, L. Myšková, V. Šmilauer, L. Alberovská, L. Vinšová,
600 Aluminosilicate polymers–influence of elevated temperatures, efflorescence, Ceramics–
601 Silikáty. 53 (2009) 276–282.

602 [23] R. Pouhet, Formulation and durability of metakaolin-based geopolymers, (2015).

603 [24] M.A. Longhi, E.D. Rodríguez, B. Walkley, Z. Zhang, A.P. Kirchheim, Metakaolin-based
604 geopolymers: Relation between formulation, physicochemical properties and
605 efflorescence formation, Compos. Part B Eng. 182 (2020) 107671.
606 https://doi.org/https://doi.org/10.1016/j.compositesb.2019.107671.

607 [25] E. Najafi Kani, A. Allahverdi, J.L. Provis, Efflorescence control in geopolymer binders
608 based on natural pozzolan, Cem. Concr. Compos. 34 (2012) 25–33.
609 https://doi.org/https://doi.org/10.1016/j.cemconcomp.2011.07.007.

[26] A. Saludung, T. Azeyanagi, Y. Ogawa, K. Kawai, Effect of silica fume on efflorescence formation and alkali leaching of alkali-activated slag, J. Clean. Prod. 315 (2021) 128210. https://doi.org/https://doi.org/10.1016/j.jclepro.2021.128210.

[27] M.A. Longhi, Z. Zhang, B. Walkley, E.D. Rodríguez, A.P. Kirchheim, Strategies for control and mitigation of efflorescence in metakaolin-based geopolymers, Cem. Concr. Res. 144 (2021) 106431. https://doi.org/https://doi.org/10.1016/j.cemconres.2021.106431.

[28] J.-B. Wang, T. Zhou, D. Xu, Z. Zhou, P. Du, N. Xie, X. Cheng, Y. Liu, Effect of nano-silica on the efflorescence of waste based alkali-activated inorganic binder, Constr. Build. Mater. 167 (2018) 381–390. https://doi.org/https://doi.org/10.1016/j.conbuildmat.2018.02.006.

[29] Y. Wang, X. Liu, W. Zhang, Z. Li, Y. Zhang, Y. Li, Y. Ren, Effects of Si/Al ratio on the efflorescence and properties of fly ash based geopolymer, J. Clean. Prod. 244 (2020) 118852. https://doi.org/https://doi.org/10.1016/j.jclepro.2019.118852.

[30] P. He, B. Zhang, S. Yang, H.A. Ali, J.-X. Lu, C.S. Poon, Recycling of glass cullet and glass powder in alkali-activated cement: Mechanical properties and alkali-silica reaction, Waste and Biomass Valorization. (2020). https://doi.org/10.1007/s12649-020-01102-5.

[31] P. Duxson, J.L. Provis, Designing precursors for geopolymer cements, J. Am. Ceram. Soc. 91 (2008) 3864–3869. https://doi.org/10.1111/j.1551-2916.2008.02787.x.

[32] J.-X. Lu, C.S. Poon, Use of waste glass in alkali activated cement mortar, Constr. Build. Mater. 160 (2018) 399–407. https://doi.org/https://doi.org/10.1016/j.conbuildmat.2017.11.080.

[33] N. Kumar, S.S. Amritphale, J.C. Matthews, J.G. Lynam, S. Alam, O.A. Abdulkareem, Synergistic utilization of diverse industrial wastes for reutilization in steel production and their geopolymerization potential, Waste Manag. 126 (2021) 728–736. https://doi.org/https://doi.org/10.1016/j.wasman.2021.04.008.

[34] A. Passuello, E.D. Rodríguez, E. Hirt, M. Longhi, S.A. Bernal, J.L. Provis, A.P. Kirchheim, Evaluation of the potential improvement in the environmental footprint of geopolymers using waste-derived activators, J. Clean. Prod. 166 (2017) 680–689.

https://doi.org/https://doi.org/10.1016/j.jclepro.2017.08.007.

[35] M. Torres-Carrasco, F. Puertas, Waste glass in the geopolymer preparation. Mechanical and microstructural characterisation, J. Clean. Prod. 90 (2015) 397–408. https://doi.org/https://doi.org/10.1016/j.jclepro.2014.11.074.

[36] M.F. Alnahhal, T. Kim, A. Hajimohammadi, Waste-derived activators for alkali-activated materials: A review, Cem. Concr. Compos. 118 (2021) 103980. https://doi.org/https://doi.org/10.1016/j.cemconcomp.2021.103980.

[37] G. Habert, J.B. d'Espinose de Lacaillerie, N. Roussel, An environmental evaluation of geopolymer based concrete production: reviewing current research trends, J. Clean. Prod. 19 (2011) 1229–1238. https://doi.org/https://doi.org/10.1016/j.jclepro.2011.03.012.

[38] Y. Alrefaei, Y.-S. Wang, J.-G. Dai, Q.-F. Xu, Effect of superplasticizers on properties of one-part Ca(OH)2/Na2SO4 activated geopolymer pastes, Constr. Build. Mater. 241 (2020) 117990. https://doi.org/https://doi.org/10.1016/j.conbuildmat.2019.117990.

[39] T.P. Wagner, Compact fluorescent lights and the impact of convenience and knowledge on household recycling rates, Waste Manag. 31 (2011) 1300–1306.

[40] EPD, Environmental Protection Department, Monitoring of solid waste in Hong Kong: Waste Statistics for 2020, (2020).

[41] C. Bobirică, J.-H. Shim, J.-H. Pyeon, J.-Y. Park, Influence of waste glass on the microstructure and strength of inorganic polymers, Ceram. Int. 41 (2015) 13638–13649.

[42] R.M. Novais, G. Ascensão, M.P. Seabra, J.A. Labrincha, Waste glass from end-of-life fluorescent lamps as raw material in geopolymers, Waste Manag. 52 (2016) 245–255. https://doi.org/https://doi.org/10.1016/j.wasman.2016.04.003.

[43] M. Cyr, R. Idir, T. Poinot, Properties of inorganic polymer (geopolymer) mortars made of glass cullet, J. Mater. Sci. 47 (2012) 2782–2797. https://doi.org/10.1007/s10853-011-6107-2.

[44] R.M. Novais, G. Ascensão, M.P. Seabra, J.A. Labrincha, Waste glass from end-of-life fluorescent lamps as raw material in geopolymers, Waste Manag. 52 (2016) 245–255.

https://doi.org/https://doi.org/10.1016/j.wasman.2016.04.003.

[45] R. Martinez-Lopez, J. Ivan Escalante-Garcia, Alkali activated composite binders of waste silica soda lime glass and blast furnace slag: Strength as a function of the composition, Constr. Build. Mater. 119 (2016) 119–129. https://doi.org/https://doi.org/10.1016/j.conbuildmat.2016.05.064.

[46] R. Xiao, Y. Zhang, X. Jiang, P. Polaczyk, Y. Ma, B. Huang, Alkali-activated slag supplemented with waste glass powder: Laboratory characterization, thermodynamic modelling and sustainability analysis, J. Clean. Prod. 286 (2021) 125554. https://doi.org/https://doi.org/10.1016/j.jclepro.2020.125554.

[47] V. Živica, Effectiveness of new silica fume alkali activator, Cem. Concr. Compos. 28 (2006) 21–25.

[48] E.D. Rodríguez, S.A. Bernal, J.L. Provis, J. Paya, J.M. Monzo, M.V. Borrachero, Effect of nanosilica-based activators on the performance of an alkali-activated fly ash binder, Cem. Concr. Compos. 35 (2013) 1–11.

[49] S.A. Bernal, E.D. Rodríguez, R.M. de Gutiérrez, J.L. Provis, S. Delvasto, Activation of metakaolin/slag blends using alkaline solutions based on chemically modified silica fume and rice husk ash, Waste and Biomass Valorization. 3 (2012) 99–108.

[50] H.K. Tchakouté, C.H. Rüscher, S. Kong, E. Kamseu, C. Leonelli, Geopolymer binders from metakaolin using sodium waterglass from waste glass and rice husk ash as alternative activators: A comparative study, Constr. Build. Mater. 114 (2016) 276–289.

[51] R. Vinai, M. Soutsos, Production of sodium silicate powder from waste glass cullet for alkali activation of alternative binders, Cem. Concr. Res. 116 (2019) 45–56. https://doi.org/https://doi.org/10.1016/j.cemconres.2018.11.008.

[52] W. Dong, W. Li, Z. Tao, A comprehensive review on performance of cementitious and geopolymeric concretes with recycled waste glass as powder, sand or cullet, Resour. Conserv. Recycl. 172 (2021). https://doi.org/10.1016/j.resconrec.2021.105664.

[53] M.H. Samarakoon, P.G. Ranjith, W. Hui Duan, A. Haque, B.K. Chen, Extensive use of waste glass in one-part alkali-activated materials: Towards sustainable construction

693 practices, Waste Manag. 130 (2021) 1–11.
694 https://doi.org/https://doi.org/10.1016/j.wasman.2021.04.060.

695 [54] M.C. Bignozzi, A. Saccani, L. Barbieri, I. Lancellotti, Glass waste as supplementary
696 cementing materials: The effects of glass chemical composition, Cem. Concr. Compos. 55
697 (2015) 45–52. https://doi.org/10.1016/j.cemconcomp.2014.07.020.

698 [55] F. Puertas, M. Torres-Carrasco, Use of glass waste as an activator in the preparation of
699 alkali-activated slag. Mechanical strength and paste characterisation, Cem. Concr. Res. 57
700 (2014) 95–104. https://doi.org/https://doi.org/10.1016/j.cemconres.2013.12.005.

701 [56] Q. Wang, J. Li, P. Tang, L. Fang, C.S. Poon, Sustainable reclamation of phosphorus from
702 incinerated sewage sludge ash as value-added struvite by chemical extraction, purification
703 and crystallization, J. Clean. Prod. 181 (2018) 717–725.
704 https://doi.org/https://doi.org/10.1016/j.jclepro.2018.01.254.

705 [57] S. Dadsetan, H. Siad, M. Lachemi, O. Mahmoodi, M. Sahmaran, Sodium glass liquid from
706 glass waste as a user-friendly hardener in structural geopolymer systems, Cem. Concr.
707 Compos. 130 (2022) 104525.
708 https://doi.org/https://doi.org/10.1016/j.cemconcomp.2022.104525.

709 [58] Z. Asadi, R. Norouzbeigi, Synthesis of colloidal nanosilica from waste glass powder as a
710 low cost precursor, Ceram. Int. 44 (2018) 22692–22697.
711 https://doi.org/https://doi.org/10.1016/j.ceramint.2018.09.050.

712 [59] H.A. Ali, D. Xuan, B. Zhang, C. Xiao, B. Zhao, Cementitious characteristics and
713 environmental behaviour of vitrified MSW incineration fly ash slag, Clean. Mater. 4
714 (2022) 100092. https://doi.org/https://doi.org/10.1016/j.clema.2022.100092.

715 [60] J.-X. Lu, P. Shen, H. Zheng, B. Zhan, H.A. Ali, P. He, C.S. Poon, Synergetic recycling of
716 waste glass and recycled aggregates in cement mortars: Physical, durability and
717 microstructure performance, Cem. Concr. Compos. (2020) 103632.
718 https://doi.org/10.1016/j.cemconcomp.2020.103632.

719 [61] S. Yang, J.-X. Lu, C.S. Poon, Recycling of waste glass in cement mortars: Mechanical
720 properties under high temperature loading, Resour. Conserv. Recycl. 174 (2021) 105831.

https://doi.org/https://doi.org/10.1016/j.resconrec.2021.105831.

[62] R. Snellings, Solution-Controlled Dissolution of Supplementary Cementitious Material Glasses at pH 13: The Effect of Solution Composition on Glass Dissolution Rates, J. Am. Ceram. Soc. 96 (2013) 2467–2475. https://doi.org/https://doi.org/10.1111/jace.12480.

[63] A. Hajimohammadi, J.S.J. van Deventer, Dissolution behaviour of source materials for synthesis of geopolymer binders: A kinetic approach, Int. J. Miner. Process. 153 (2016) 80–86. https://doi.org/https://doi.org/10.1016/j.minpro.2016.05.014.

[64] H. Maraghechi, F. Rajabipour, C.G. Pantano, W.D. Burgos, Effect of calcium on dissolution and precipitation reactions of amorphous silica at high alkalinity, Cem. Concr. Res. 87 (2016) 1–13. https://doi.org/10.1016/j.cemconres.2016.05.004.

[65] H.A. Ali, D. Xuan, C.S. Poon, Assessment of long-term reactivity of initially lowly-reactive solid wastes as supplementary cementitious materials (SCMs), Constr. Build. Mater. 232 (2020). https://doi.org/10.1016/j.conbuildmat.2019.117192.

[66] M. Lahoti, K.K. Wong, K.H. Tan, E.-H. Yang, Effect of alkali cation type on strength endurance of fly ash geopolymers subject to high temperature exposure, Mater. Des. 154 (2018) 8–19. https://doi.org/https://doi.org/10.1016/j.matdes.2018.05.023.

[67] M.B. Ogundiran, S. Kumar, Synthesis and characterisation of geopolymer from Nigerian Clay, Appl. Clay Sci. 108 (2015) 173–181. https://doi.org/https://doi.org/10.1016/j.clay.2015.02.022.

[68] C.R. Kaze, T. Alomayri, A. Hasan, S. Tome, G.L. Lecomte-Nana, J.G.D. Nemaleu, H.K. Tchakoute, E. Kamseu, U.C. Melo, H. Rahier, Reaction kinetics and rheological behaviour of meta-halloysite based geopolymer cured at room temperature: Effect of thermal activation on physicochemical and microstructural properties, Appl. Clay Sci. 196 (2020) 105773. https://doi.org/https://doi.org/10.1016/j.clay.2020.105773.

[69] Y. Ling, K. Wang, X. Wang, S. Hua, Effects of mix design parameters on heat of geopolymerization, set time, and compressive strength of high calcium fly ash geopolymer, Constr. Build. Mater. 228 (2019) 116763. https://doi.org/https://doi.org/10.1016/j.conbuildmat.2019.116763.

[70] T. Seiffarth, M. Hohmann, K. Posern, C. Kaps, Effect of thermal pre-treatment conditions of common clays on the performance of clay-based geopolymeric binders, Appl. Clay Sci. 73 (2013) 35–41. https://doi.org/https://doi.org/10.1016/j.clay.2012.09.010.

[71] S. Kumar, R. Kumar, T.C. Alex, A. Bandopadhyay, S.P. Mehrotra, Influence of reactivity of fly ash on geopolymerisation, Adv. Appl. Ceram. 106 (2007) 120–127. https://doi.org/10.1179/174367607X159293.

[72] P. Suraneni, J. Weiss, Examining the pozzolanicity of supplementary cementitious materials using isothermal calorimetry and thermogravimetric analysis, Cem. Concr. Compos. 83 (2017) 273–278. https://doi.org/https://doi.org/10.1016/j.cemconcomp.2017.07.009.

[73] Y. Alrefaei, Y.-S. Wang, J.-G. Dai, The effectiveness of different superplasticizers in ambient cured one-part alkali activated pastes, 97 (2019) 166–174.

[74] Y. Alrefaei, Y.-S. Wang, J.-G. Dai, Effect of mixing method on the performance of alkali-activated fly ash/slag pastes along with polycarboxylate admixture, Cem. Concr. Compos. 117 (2021) 103917. https://doi.org/https://doi.org/10.1016/j.cemconcomp.2020.103917.

[75] ASTM C109, Standard test method for compressive strength of hydraulic cement mortars (Using 2-in. or [50 mm] cube specimens), (2020).

[76] B. Grambow, Corrosion of glass, Uhlig's Corros. Handb. 51 (2011) 399.

[77] Y. Liu, C. Shi, Z. Zhang, N. Li, An overview on the reuse of waste glasses in alkali-activated materials, Resour. Conserv. Recycl. 144 (2019) 297–309. https://doi.org/https://doi.org/10.1016/j.resconrec.2019.02.007.

[78] F.H. El-Batal, E.M. Khalil, Y.M. Hamdy, H.M. Zidan, M.S. Aziz, A.M. Abdelghany, FTIR spectral analysis of corrosion mechanisms in soda lime silica glasses doped with transition metal oxides, Silicon. 2 (2010) 41–47. https://doi.org/10.1007/s12633-010-9037-8.

[79] J. Wong, C.A. Angell, Glass: Structure by spectroscopy, Marcel Dekker Inc., New York. (1976) 864.

776 [80] D. Dimas, I. Giannopoulou, D. Panias, Polymerization in sodium silicate solutions: a
777 fundamental process in geopolymerization technology, J. Mater. Sci. 44 (2009) 3719–
778 3730. https://doi.org/10.1007/s10853-009-3497-5.

779 [81] Y.-K. Lee, Y.L. Peng, M. Tomozawa, IR reflection spectroscopy of a soda-lime glass
780 surface during ion-exchange, J. Non. Cryst. Solids. 222 (1997) 125–130.
781 https://doi.org/https://doi.org/10.1016/S0022-3093(97)90104-6.

782 [82] R.W. Douglas, T.M.M. El-Shamy, Reactions of glasses with aqueous solutions, J. Am.
783 Ceram. Soc. 50 (1967) 1–8.

784 [83] F. Puertas, A. Fernández-Jiménez, Mineralogical and microstructural characterisation of
785 alkali-activated fly ash/slag pastes, Cem. Concr. Compos. 25 (2003) 287–292.
786 https://doi.org/https://doi.org/10.1016/S0958-9465(02)00059-8.

787 [84] S. Zhang, A. Keulen, K. Arbi, G. Ye, Waste glass as partial mineral precursor in alkali-
788 activated slag/fly ash system, Cem. Concr. Res. 102 (2017) 29–40.

789 [85] F. Puertas, S. Martínez-Ramírez, S. Alonso, T. Vázquez, Alkali-activated fly ash/slag
790 cements: strength behaviour and hydration products, Cem. Concr. Res. 30 (2000) 1625–
791 1632.

792 [86] N.J. Clayden, S. Esposito, A. Aronne, P. Pernice, Solid state 27Al NMR and FTIR study
793 of lanthanum aluminosilicate glasses, J. Non. Cryst. Solids. 258 (1999) 11–19.
794 https://doi.org/https://doi.org/10.1016/S0022-3093(99)00555-4.

795 [87] M. Criado, A. Fernández-Jiménez, A. Palomo, Alkali activation of fly ash: Effect of the
796 SiO2/Na2O ratio: Part I: FTIR study, Microporous Mesoporous Mater. 106 (2007) 180–
797 191. https://doi.org/https://doi.org/10.1016/j.micromeso.2007.02.055.

798 [88] I. García-Lodeiro, A. Fernández-Jiménez, D.E. Macphee, I. Sobrados, J. Sanz, A. Palomo,
799 Stability of synthetic calcium silicate hydrate gels in presence of alkalis, aluminum, and
800 soluble silica, Transp. Res. Rec. 2142 (2010) 52–57. https://doi.org/10.3141/2142-08.

801 [89] R. Redden, N. Neithalath, Microstructure, strength, and moisture stability of alkali
802 activated glass powder-based binders, Cem. Concr. Compos. 45 (2014) 46–56.
803 https://doi.org/https://doi.org/10.1016/j.cemconcomp.2013.09.011.

[90] P. He, B. Zhang, J.-X. Lu, C.S. Poon, A ternary optimization of alkali-activated cement mortars incorporating glass powder, slag and calcium aluminate cement, Constr. Build. Mater. 240 (2020) 117983. https://doi.org/https://doi.org/10.1016/j.conbuildmat.2019.117983.

[91] X. Dai, S. Aydın, M.Y. Yardımcı, K. Lesage, G. De Schutter, Rheology and microstructure of alkali-activated slag cements produced with silica fume activator, Cem. Concr. Compos. 125 (2022) 104303. https://doi.org/https://doi.org/10.1016/j.cemconcomp.2021.104303.

[92] X. Dai, S. Aydin, M.Y. Yardimci, K. Lesage, G. de Schutter, Influence of water to binder ratio on the rheology and structural Build-up of Alkali-Activated Slag/Fly ash mixtures, Constr. Build. Mater. 264 (2020) 120253. https://doi.org/https://doi.org/10.1016/j.conbuildmat.2020.120253.

[93] F. Puertas, M. Palacios, H. Manzano, J.S. Dolado, A. Rico, J. Rodríguez, A model for the CASH gel formed in alkali-activated slag cements, J. Eur. Ceram. Soc. 31 (2011) 2043–2056.

[94] T. Liu, Q. Yu, H.J.H. Brouwers, X. Fan, Utilization of waste glass in alkali activated slag/fly ash blends: reaction process, microstructure, and chloride diffusion behavior, J. Sustain. Cem. Mater. (2022) 1–11. https://doi.org/10.1080/21650373.2022.2082577.

[95] S.C. Kohn, R. Dupree, M.E. Smith, Proton environments and hydrogen-bonding in hydrous silicate glasses from proton NMR, Nature. 337 (1989) 539–541.

[96] D.E. Clark, M.F. Dilmore, E.C. Ethridge, L.L. Hench, Aqueous corrosion of soda-silica and soda-lime-silica glass, J. Am. Ceram. Soc. 59 (1976) 62–65.

[97] H. Scholze, Glass-water interactions, J. Non. Cryst. Solids. 102 (1988) 1–10. https://doi.org/https://doi.org/10.1016/0022-3093(88)90105-6.